

RAPID COMMUNICATION | SEPTEMBER 18 2023

A new method for reactive constant pH simulations **FREE**

Yan Levin   ; Amin Bakhshandeh 



J. Chem. Phys. 159, 111101 (2023)

<https://doi.org/10.1063/5.0166840>



CrossMark

Articles You May Be Interested In

Donnan phenomena in membranes with charge due to ion adsorption. Effects of the interaction between adsorbed charged groups

J. Chem. Phys. (February 1993)

pH and salt concentration dependence of the microstructure of poly(N-isopropylacrylamide-co-acrylic acid) gels

J. Chem. Phys. (September 1996)

Repulsive and attractive depletion forces mediated by nonadsorbing polyelectrolytes in the Donnan limit

J. Chem. Phys. (April 2021)

500 kHz or 8.5 GHz?
And all the ranges in between.

Lock-in Amplifiers for your periodic signal measurements



Find out more



A new method for reactive constant pH simulations

Cite as: J. Chem. Phys. 159, 111101 (2023); doi: 10.1063/5.0166840

Submitted: 7 July 2023 • Accepted: 29 August 2023 •

Published Online: 18 September 2023



View Online



Export Citation



CrossMark

Yan Levin^{a)}  and Amin Bakhshandeh 

AFFILIATIONS

Instituto de Física, Universidade Federal do Rio Grande do Sul, Caixa Postal 15051, CEP 91501-970 Porto Alegre, RS, Brazil

^{a)} Author to whom correspondence should be addressed: levin@if.ufrgs.br

ABSTRACT

We present a simulation method that allows us to calculate the titration curves for systems undergoing protonation/deprotonation reactions—such as charged colloidal suspensions with acidic/basic surface groups, polyelectrolytes, polyampholytes, and proteins. The new approach allows us to simultaneously obtain titration curves both for systems in contact with salt and acid reservoir (semi-grand canonical ensemble) and for isolated suspensions (canonical ensemble). To treat the electrostatic interactions, we present a new method based on Ewald summation—which accounts for the existence of both Bethe and Donnan potentials within the simulation cell. We show that the Donnan potential dramatically affects the pH of a suspension. Counterintuitively, we find that in suspensions with a large volume fraction of nanoparticles and low ionic strength, the number of deprotonated groups can be 100% larger in an isolated system, compared to a system connected to a reservoir by a semi-permeable membrane—both systems being at *exactly* the same pH.

Published under an exclusive license by AIP Publishing. <https://doi.org/10.1063/5.0166840>

In many physics, chemistry, and biology applications, one needs to understand systems with active surface groups.^{1–16} Depending on the pH and salt concentration inside the solution, a surface group can be either protonated or deprotonated.^{3,17–21} The state in which a group finds itself depends on its intrinsic acid dissociation constant, the local concentration of hydronium ions, the electrostatic potential in the vicinity of the group, the steric repulsion between ions, etc. For some simple surfaces—such as metal oxide or colloidal particles with regular arrangement of surface groups, it is possible to develop a theoretical approach, which can fairly accurately predict the resulting surface charge and its dependence on salt and pH inside the solution.^{22–25} Unfortunately, no purely theoretical approach is possible for more complex systems, such as polyelectrolytes or proteins. Furthermore, even in the case of simple surfaces in solutions containing multivalent ions, one finds that theoretical approaches begin to fail.^{26,27} For such complex systems, one is forced to rely on computer simulations.^{19,28–30} The constant pH (cpH) simulation method is the most popular tool to obtain titration curves of such systems.^{31,32} There is, however, a fundamental difficulty in using such an approach indiscriminately. In cpH simulations, proteins, colloidal particles, or polyelectrolytes are confined inside a simulation box, while ions can be freely exchanged with the reservoir of acid and salt.^{33–35} The cpH simulation method is,

therefore, intrinsically semi-grand canonical.³⁰ When performing a cpH simulation, a proton is implicitly brought into the system from an external reservoir at a fixed pH. To keep the charge neutrality inside the simulation cell, one of the cations or protons inside the bulk of the cell is arbitrarily deleted. However, such an arbitrary deletion does not respect the detailed balance and leads to incorrect results, unless the system contains a lot of salt and is very dilute in polyelectrolyte.^{28,30} Fortunately, it is easy to correct the standard cpH algorithm by combining a protonation move with a simultaneous grand canonical insertion of an anion and a deprotonation move with a simultaneous grand canonical deletion of an anion.^{19,28–30,36,37} This restores the detailed balance of the cpH algorithm, making it internally consistent. This corrected version of the cpH algorithm will be used in the present Communication.

In a real physical system, to confine polyelectrolytes or colloidal particles within some region of space requires a semi-permeable membrane, which would separate the system from the reservoir containing acid and salt. Since the counterions are at larger concentration inside the system than they are in the reservoir, they will tend to diffuse across the membrane.³⁸ The net ionic flux will end when a sufficiently large electrostatic potential difference is established between the reservoir and the system, forcing the reversal of the flow. This is known as the Donnan potential.^{39,40} In fact, one does

not need to have a membrane to establish a finite Donnan potential. For example, a colloidal column in a gravitational field^{41–43} will spontaneously establish a finite Donnan potential along the vertical direction. This happens because, in general, colloidal particles have a finite buoyant mass,^{44,45} which forces them to be inhomogeneously distributed inside the suspension. Meanwhile, the ions are not affected by the gravitational field and are free to diffuse throughout all space, including the top portion of suspension, where there are no colloidal particles. This results in Donnan potential along the vertical direction of colloidal suspension. In this case, the gravitational field plays the role similar to that of a membrane, separating the region in which colloidal particles can be found. The important point that is often lost when performing constant pH simulations is that the systems (simulation cell) are always at a different electrostatic potential from the reservoir. Meanwhile, the electrochemical potentials and, consequently, the pH inside the system and the reservoir are the same.

Recall that pH of a solution is defined in terms of activity of hydronium ions, $\text{pH} = -\log_{10}[a_+/c^\ominus]$, where $c^\ominus = 1\text{M}$ is the standard concentration. On the one hand, inside the reservoir, the activity of hydronium ions is $a_+ = c_{\text{H}^+} \exp(\beta\mu_{\text{ex}}^r)$, where c_{H^+} is the concentration of hydronium ions inside the reservoir and μ_{ex}^r is their excess chemical potential. On the other hand, inside the system, $a_+ = \rho_{\text{H}^+} \exp[\beta\mu_{\text{ex}}^s + q\beta\varphi_D]$, where q is the proton charge, ρ_{H^+} is the concentration of hydronium ions inside the system, and φ_D is the Donnan potential difference between the reservoir and the system. Note that the concentration of hydronium ions inside the system is different from their concentration inside the reservoir. Furthermore, while inside the reservoir, μ_{ex}^r is due only to the interaction between the ions, inside the system, μ_{ex}^s also includes contributions coming from electrostatic and steric interactions of hydronium ions with the colloidal particles. Nevertheless, equivalence between electrochemical potentials inside the system and the reservoir requires that pH of both be the same. (For the additional discussion of the definition of pH in inhomogeneous systems see the Conclusions of this Communication.) We see the important role that the Donnan potential plays for determining pH inside a system that is in contact with a reservoir. If one uses hydrogen and calomel (reference) electrodes to measure pH inside a system connected to a reservoir by a semi-permeable membrane—with calomel placed in the reservoir—the Donnan potential will be an integral part of the measurement. Suppose now that the system is equilibrated and then disconnected from the reservoir—so that the number of ions of each type remains fixed and no longer fluctuates. Clearly based on the ensemble equivalence of statistical mechanics, the number of protonated groups in such a canonical system will remain exactly the same as in the original semi-grand canonical system. However, the pH of such a canonical system will no longer be the same as that of the semi-grand canonical system connected to the reservoir. The reason for this is that inside a canonical system, the potential drop between system and reservoir will no longer exist and the activity of hydronium ions will be $a_+ = \rho_{\text{H}^+} \exp[\beta\mu_{\text{ex}}^s]$. Substituting this into the definition of pH, we find the relation between the canonical and grand canonical pH,

$$\text{pH}_c = \text{pH}_{gc} + \frac{\beta\varphi_D}{\ln(10)}. \quad (1)$$

Equation (1) opens a way for us to use the grand-canonical Monte Carlo (GCMC) simulation to simultaneously calculate titration curves for both canonical and grand-canonical systems. However, to do this, the usual GCMC algorithm, which relies on cation–anion pair insertion into the simulation cell, in order to preserve the charge neutrality, must be modified to allow for the charge fluctuation inside the cell, in order to calculate the Donnan potential. Note that the Donnan potential is not accessible in the normal GCMC since it cancels out for pair moves involving oppositely charged particles. In this Communication, we will present a reactive GCMC–Donnan (rGCMCD) simulation method, which will allow us to calculate the number of protonated groups and the Donnan potential in a single simulation. Combining this with Eq. (1), we are able to obtain the number of protonated group for a given pH in both canonical and grand-canonical systems. We should stress that at this time, there is no alternative method that permits us to calculate titration curves for isolated (canonical) systems. In principle, one could use canonical reactive MC simulations and then attempt to use the Widom insertion method to obtain the excess chemical potential of hydronium ions inside the simulation cell. The problem, however, is that for moderate and large pH, there might not be any hydronium ions inside the simulation cell, thus preventing us from obtaining an accurate canonical pH.

The difficulty in performing simulations of Coulomb systems stems from the long range electrostatic interaction between the particles that cannot be cut off at the cell boundary. Instead, one is forced to periodically replicate the whole simulation cell so that a given ion interacts not only with the ions inside the cell but also with their infinite replicas. For Donnan simulations presented in this Communication, there is an additional difficulty because the simulation cell is no longer charge neutral. The total charge inside the cell, $Q_t = \sum_i q_i$, where the sum is over all the ions and the charged groups, is not necessarily zero at a given instant of simulation. Clearly, such an imbalance of charge in an infinitely replicated system leads to the divergence of the electrostatic energy. To avoid this, we introduce a uniform neutralizing background of charge density $\rho_b = -Q_t/V$, where V is the volume of the simulation cell. The charge density inside the system can then be written as

$$\rho_q(\mathbf{r}) = \sum_i q_i \delta(\mathbf{r} - \mathbf{r}_i) - \frac{Q_t}{V}. \quad (2)$$

Using the usual approach, the electrostatic potential can be split into long and short range contribution.^{46–48} The long range can be efficiently summed in the Fourier space, while the short range is summed in the real space,^{49–51} resulting in the electrostatic potential at position \mathbf{r} inside the simulation cell,

$$\begin{aligned} \varphi(\mathbf{r}) = & \sum_{\mathbf{k}=0}^{\infty} \sum_{j=1}^N \frac{4\pi q^j}{\epsilon_w V |\mathbf{k}|^2} \exp\left[-\frac{|\mathbf{k}|^2}{4\kappa_c^2} + i\mathbf{k} \cdot (\mathbf{r} - \mathbf{r}^j)\right] \\ & + \sum_{j=1}^N \sum_{\mathbf{n}} q^j \frac{\text{erfc}(\kappa_c |\mathbf{r} - \mathbf{r}^j - L\mathbf{n}|)}{\epsilon_w |\mathbf{r} - \mathbf{r}^j - L\mathbf{n}|} \\ & + \frac{1}{V} \sum_{\mathbf{k}=0}^{\infty} \tilde{\varphi}_b(\mathbf{k}) \exp[i\mathbf{k} \cdot \mathbf{r}], \end{aligned} \quad (3)$$

where $\mathbf{n} = (n_1, n_2, n_3)$ are integers, $\mathbf{k} = (\frac{2\pi}{L}n_1, \frac{2\pi}{L}n_2, \frac{2\pi}{L}n_3)$ are the reciprocal lattice vectors, and κ_c is an arbitrary damping parameter.

The last term is the electrostatic potential due to the uniform background, of which the Fourier transform is

$$\tilde{\varphi}_b(\mathbf{k}) = -\frac{4\pi Q_t}{\epsilon_w V} \frac{\int_V e^{-i\mathbf{k}\cdot\mathbf{r}} d^3r}{k^2}. \quad (4)$$

Note that the electrostatic potential, Eq. (A1), is invariant to the specific value of the damping parameter κ_e . It is usual to choose κ_e sufficiently large so that simple periodic boundary conditions can be used for the short range part of the electrostatic potential.

The limit $\mathbf{k} \rightarrow 0$ in the Fourier sum of Eq. (A1) is singular and must be performed with great care. The limiting procedure is shown in Appendix A, where we obtain

$$\begin{aligned} \varphi(\mathbf{r}) = & \sum_{\mathbf{k} \neq 0} \sum_{j=1}^N \frac{4\pi q^j}{\epsilon_w V |\mathbf{k}|^2} \exp \left[-\frac{|\mathbf{k}|^2}{4\kappa_e^2} + i\mathbf{k} \cdot (\mathbf{r} - \mathbf{r}^j) \right] \\ & + \sum_{j=1}^N \sum_n q^j \frac{\text{erfc}(\kappa_e |\mathbf{r} - \mathbf{r}^j - L\mathbf{n}|)}{\epsilon_w |\mathbf{r} - \mathbf{r}^j - L\mathbf{n}|} \\ & - \frac{\pi Q_t}{\epsilon_w V \kappa_e^2} + \frac{4\pi}{3\epsilon_w V} \mathbf{r} \cdot \mathbf{M} + \phi_B, \end{aligned} \quad (5)$$

where $\mathbf{M} = \sum_i q_i \mathbf{r}_i$ is the electric dipole moment inside the cell and ϕ_B is the modified Bethe potential of the cell with a neutralizing background,

$$\phi_B = -\frac{2\pi}{3\epsilon_w V} \sum_i q_i r_i^2 + \frac{\pi Q_t}{6\epsilon_w L}. \quad (6)$$

We recognize the \mathbf{M} dependent term in Eq. (A13) as arising from the uniform polarization of the macroscopic crystal composed of spherically replicated simulation cells. From continuum electrostatics, such uniform polarization is equivalent to the surface charge density $\mathbf{M} \cdot \mathbf{n}/V$, where \mathbf{n} is the unit normal to the boundary of the macroscopic spherical crystal, resulting in an electrostatic potential $\frac{4\pi}{3\epsilon_w V} \mathbf{r} \cdot \mathbf{M}$ in the interior of the crystal; see Fig. 1.

The nature of ϕ_B is more subtle. In general, a simulation cell containing colloidal particles or polyelectrolytes will have a non-zero trace of the second moment charge density tensor. Spherical replication of such cells will lead to a crystal with a dipole surface layer,⁵² across which there will be a potential drop precisely given by Eq. (6). In Appendix B, we also provide an alternative real space derivation of Eq. (6).

Since ions can diffuse across the membrane, while colloidal particles are confined within the system, a Donnan potential exists between the reservoir and the system. While the Bethe potential can be thought of as the average of the local electrostatic potential inside the periodically replicated crystal, the Donnan potential is inherently an interfacial effect that arises from ionic diffusion between the system and the reservoir. The total electrostatic potential drop between the system and the reservoir is shown in Fig. 2.

The electrostatic energy can be calculated using

$$\begin{aligned} E = & \frac{1}{2} \int \rho_q(\mathbf{r}) \varphi(\mathbf{r}) d^3r \\ = & \frac{1}{2} \sum_i q_i \lim_{\mathbf{r} \rightarrow \mathbf{r}_i} \left[\varphi(\mathbf{r}) - \frac{q_i}{\epsilon_w |\mathbf{r} - \mathbf{r}_i|} \right] \\ & - \frac{Q_t}{2V} \lim_{\mathbf{k} \rightarrow 0} \tilde{\varphi}(\mathbf{k}). \end{aligned} \quad (7)$$

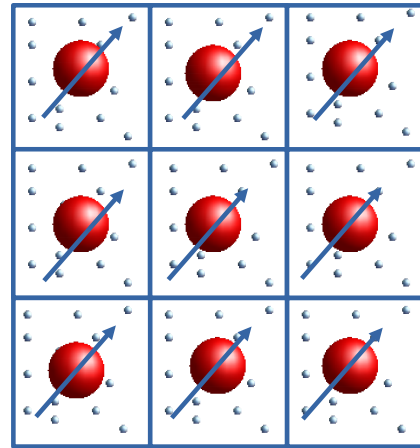


FIG. 1. Replicas of the simulation cell. The large sphere is a colloidal particle and the small spheres are ions; the arrows show the instantaneous electric dipole moment \mathbf{M} , which, in general, exists inside the cell. Furthermore, the trace of the instantaneous second moment charge distribution tensor of a locally strongly inhomogeneous system of colloidal particles and ions will not be zero. A macroscopic spherical crystal produced by a periodic replication of the simulation cell will then have both surface charge density $\mathbf{M} \cdot \mathbf{n}/V$ and a dipolar layer, which results in a potential drop across the crystal–reservoir interface, given by the modified Bethe potential, ϕ_B .

The subtraction inside the square brackets eliminates the self-energy contribution to the total electrostatic energy of all ions and charged groups. The last term is due to the background charge. Noting that the electrostatic energy is invariant with the damping parameter κ_e , the limit in the last term can be calculated using $\kappa_e \rightarrow \infty$, which kills off the real space sum in Eq. (A13). Taking the limit $\lim_{\mathbf{k} \rightarrow 0}$, the

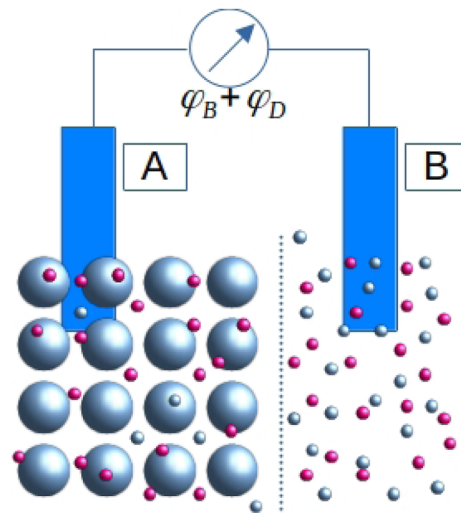


FIG. 2. Periodically replicated system separated from the reservoir by a semi-permeable membrane: the electrostatic potential difference between the two is $\phi_B + \varphi_D$.

last term of Eq. (7) then evaluates to $Q_i \phi_B / 2$ and the total electrostatic energy of a system with ions + sites of total charge Q_t and a neutralizing background can be written as

$$E = \frac{1}{2} \sum_{ij}' \sum_{\mathbf{n}} \frac{q_i q_j \operatorname{erfc}(\kappa_e |\mathbf{r}_i - \mathbf{r}_j - L\mathbf{n}|)}{\epsilon_w |\mathbf{r}_i - \mathbf{r}_j - L\mathbf{n}|} + \sum_{\mathbf{k} \neq 0} \frac{2\pi \exp(-\mathbf{k}^2 / 4\kappa_e)}{\epsilon_w V \mathbf{k}^2} (A(\mathbf{k})^2 + B(\mathbf{k})^2) - \sum_i \frac{q_i^2 \kappa_e}{\epsilon_w \sqrt{\pi}} - \frac{\pi Q_t^2}{2\epsilon_w V \kappa_e^2} + \frac{2\pi}{3\epsilon_w V} M^2, \quad (8)$$

where

$$A(\mathbf{k}) = \sum_i q_i \cos(\mathbf{k} \cdot \mathbf{r}_i), \quad (9)$$

$$B(\mathbf{k}) = \sum_i q_i \sin(\mathbf{k} \cdot \mathbf{r}_i),$$

and the prime on the sum indicates that $i = j$ is excluded from the summation when $\mathbf{n} = 0$. Note that the Bethe potential canceled out and does not contribute to the total electrostatic energy. Furthermore, since the system is implicitly connected to a reservoir, it is not possible to use the tinfoil boundary condition,⁵³—which would eliminate $\mathbf{k} = 0$ term from the Ewald summation, isolating the system from the reservoir.

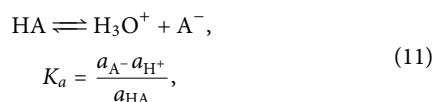
The simulation involves individual insertion/deletion moves, as well as protonation and deprotonation moves. For an ion of charge q_i to enter the simulation cell, it must cross the macroscopic boundary of the crystal. This will result in electrostatic energy change $q_i(\varphi_D + \phi_B)$. The grand canonical acceptance probabilities for insertion/deletion moves can then be written as $\min(1, \phi_{add/rem})$, where $\phi_{add/rem}$ is

$$\phi_{add} = \frac{c^\ominus V 10^{-pX_i}}{N_i + 1} e^{-\beta(\Delta E_{ele} + q_i[\varphi_D + \phi_B])}, \quad (10)$$

$$\phi_{rem} = \frac{N_i 10^{pX_i}}{V c^\ominus} e^{-\beta(\Delta E_{ele} - q_i[\varphi_D + \phi_B])},$$

where ΔE_{ele} is the change in electrostatic energy upon insertion/deletion of ion of type i and $pX_i \equiv -\log_{10} X_i / c^\ominus$, in which X_i is the activity of ion i inside the reservoir. To relate pX_i to the concentration of salt, one can perform a separate GCMC simulation for the reservoir. In practice, however, we find that for monovalent ions, the mean spherical approximation (MSA) combined with the Carnahan–Starling (CS) expression for the excluded volume^{54,55} provides an excellent approximation for the relation between pX_i , pH , and the concentrations of salt and acid in the reservoir.

The protonation/deprotonation moves involve a reaction,



where A^- is the deprotonated site. We recognize the acid dissociation constant to be the inverse of the internal partition function of HA molecule. The free energy change due to the removal of hydro-

nium from the reservoir and its reaction with an *isolated* A^- group is then

$$\beta \Delta F_p = \ln \left(\frac{K_a}{c^\ominus} \right) - \mu_{\text{H}^+}, \quad (12)$$

where $\mu_{\text{H}^+} = \ln(c_{\text{H}^+} / c^\ominus) + \beta \mu_{ex}$ is the total chemical potential of a hydronium ion inside the reservoir. For the deprotonation reaction, the free energy change is reversed so that $\Delta F_d = -\Delta F_p$. The acceptance probabilities for protonation and deprotonation moves are then $\min(1, \phi_{p/d})$, where

$$\phi_p = e^{-\beta(\Delta E_{ele} + \Delta F_p + q[\varphi_D + \phi_B])} = 10^{pK_a - pH_a} e^{-\beta(\Delta E_{ele} + q[\varphi_D + \phi_B])}, \quad (13)$$

$$\phi_d = e^{-\beta(\Delta E_{ele} + \Delta F_d - q[\varphi_D + \phi_B])} = 10^{pH - pK_a} e^{-\beta(\Delta E_{ele} - q[\varphi_D + \phi_B])}.$$

We have defined the intrinsic pK_a of a titration site as $pK_a = -\log_{10}[K_a / c^\ominus]$. During the protonation/deprotonation moves, a titration site is randomly chosen and its state is changed with an acceptance probability given by Eq. (13).

The simulation starts with an initial guess for the value of φ_D . After each MC step, the Donnan potential is automatically updated so as to drive the system toward a charge neutral state, $\varphi_D^{new} := \varphi_D^{old} + \alpha Q_t$, where $\alpha > 0$ is an arbitrary small parameter that controls convergence. The simulation stops when $\langle Q_t \rangle \approx 0$, to the desired accuracy. In practice, the system very quickly converges to a state in which Q_t has small oscillations about zero. To make sure that the system is fully equilibrated, we monitor the energy. When $\langle E \rangle$ becomes constant, we know that the system has reached equilibrium. Usually, we use 5×10^6 particle moves for equilibration. After this, we collect samples, which include colloidal charge, Donnan potential, and ion distribution. The samples are collected with intervals of ~ 3000 particle moves, to make sure that they are fully uncorrelated. We use 20 000 such samples to calculate the averages.

As an example of the algorithm developed in the present Communication, we will use it to study a colloidal suspension of finite volume fraction. The colloidal particles have radius 60 Å and contain $Z = 600$ active surface groups of intrinsic $pK_a = 5.4$ uniformly distributed over the surface. All ions have radius 2 Å, and the solvent is modeled as a dielectric continuum of Bjerrum length, $\lambda_B = q^2 / \epsilon k_B T = 7.2$ Å. The reservoir contains acid of an arbitrary pH and 1:1 salt of concentration 1 mM. The electrostatic energy is calculated using Eq. (A11), with the damping parameter set to $\kappa_e = 5/L$, where L is the size of the cubic simulation box. Such a value of κ_e is sufficiently large that simple periodic boundary conditions can be used to evaluate the short range (sum over erfc) contribution to the electrostatic energy in Eq. (A11).

For simplicity, in the present Communication, we will use only one colloidal particle inside a cubic simulation box of $L = 200$ Å. There is, however, no conceptual difficulty in using an arbitrary number of colloidal particles inside a simulation box, except for the CPU time constraint. Finally, to test the new rGCMCD algorithm, we perform a “standard” cpH in which a protonation

move is combined with a grand canonical insertion of anion and a deprotonation move with a grand canonical deletion of an anion.^{28,30,56} The acceptance probabilities for these pair moves are, respectively,

$$P_p = \min \left[1, \frac{c^\ominus V 10^{\text{pK}_a - \text{pH} - \text{pCl}}}{N_{\text{Cl}} + 1} e^{-\beta \Delta E} \right],$$

$$P_d = \min \left[1, \frac{N_{\text{Cl}} 10^{\text{pH} - \text{pK}_a + \text{pCl}}}{c^\ominus V} e^{-\beta \Delta E} \right]. \quad (14)$$

Since both Bethe and Donnan potentials cancel out in the pair moves, cpH simulation does not permit us to calculate the canonical titration curve. Meanwhile, the grand-canonical curve obtained using the “standard” cpH must agree precisely with the one obtained using our new rGCMCD simulation method. This is exactly what is found, validating the rGCMCD method.

In Fig. 3, we present the titration curves obtained using our rGCMCD simulations for both canonical (isolated) and semi-grand canonical suspensions.

As can be seen from the figure, there is a very significant difference between titration curves of an isolated colloidal suspension and those of suspension connected to a salt and acid reservoir. For example, at pH = 7.5, 28% of surface groups of semi-grand canonical system are deprotonated, while for an isolated canonical system, this jumps to 57%. When the concentration of salt increases, the difference between canonical and semi-grand canonical systems

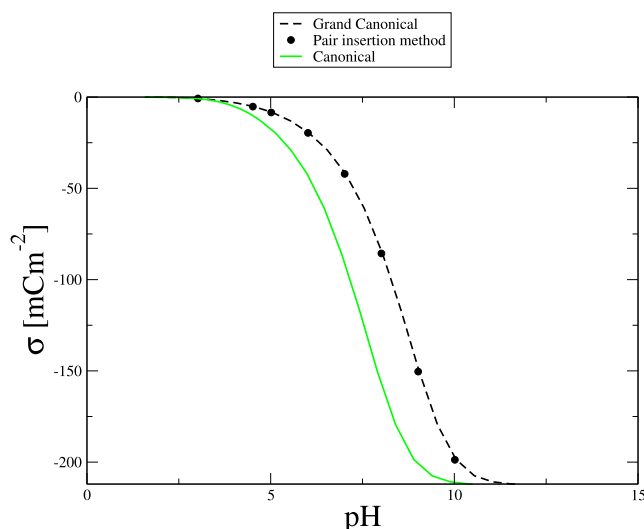


FIG. 3. Titration curves for an isolated (canonical, solid curve) and semi-grand canonical system (dashed curve) in contact with a salt and acid reservoir, calculated using rGCMCD simulations. In the semi-grand canonical case, the reservoir contains 1 mM of salt; for the canonical case, the concentration in reservoir is fine-tuned so that there is 1 mM of salt inside the system for all pH. This, however, has an imperceptible effect on the canonical titration curve for low salt concentrations. The dots are the results of the “standard” cpH with pair insertions, which agree perfectly with the new rGCMCD method. The colloidal suspension has a volume fraction of 11.3%. The saturated colloidal charge is -212 mCm^{-2} . The pK_a of acidic groups is 5.4.

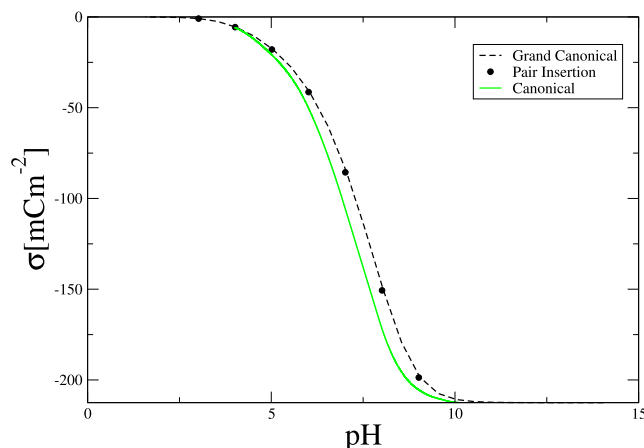


FIG. 4. Titration curves for an isolated (canonical, solid curve) and semi-grand canonical system (dashed curve) in contact with a salt and acid reservoir, calculated using rGCMCD simulations. In the semi-grand canonical case, the reservoir contains 10 mM of salt; for the canonical case, the concentration in reservoir is fine-tuned so that there is 10 mM of salt inside the system for all pH. The dots are the results of cpH pair insertion simulation. The colloidal suspension has a volume fraction of 11.3%. The saturated colloidal surface charge is -212 mCm^{-2} . The pK_a of acidic groups is 5.4.

diminishes; see Fig. 4. This justifies the use of cpH methods to study biologically relevant systems that contain physiological concentrations of salt of $c_s \approx 150 \text{ mM}$, which are usually isolated from any external reservoir.

We have presented a new simulation method that enables us to simultaneously obtain titration curves for both isolated systems (canonical ensemble) and systems connected to an external reservoir by a semi-permeable membrane. Counterintuitively, we find that at low ionic strength, the number of deprotonated groups can be 100% larger in an isolated system, compared to a system connected to a reservoir by a semi-permeable membrane—both systems at exactly the same pH! The difference can be even greater for more concentrated (large colloidal volume fraction) suspensions in deionized solutions. As the concentration of salt increases, the difference between the ensembles becomes less important, justifying the use of cpH methods for studying biologically relevant systems that are usually closed and contain large concentrations of salt. It is important to stress that at the moment there is no alternative method available to study canonical systems at moderate and high pH. The usual canonical reactive simulations fail under such conditions since the simulation cell contains none or very few hydronium ions, preventing one from accurately calculating the pH inside the system.

In our definition of pH for heterogeneous systems, we have followed the Gibbs–Guggenheim principle,⁵⁷ which prohibits the separation of the electrochemical potential into chemical and electrostatic potential contributions for the definition of measurable quantities. Meanwhile, in the electrochemistry literature, the Gibbs–Guggenheim principle is often disregarded and pH is defined in terms of only the chemical part of the total electrochemical potential. From the practical point of view, pH is determined by measuring the electromotive force (EMF) between a glass or hydrogen electrode

and a saturated calomel (reference) electrode. In our definition of pH, the reference electrode is always kept inside the reservoir, while the hydrogen electrode is moved between the reservoir and the system. With this setup, we will obtain the same EMF independent of the position of the hydrogen electrode, indicating the same pH inside the system and in the reservoir.⁵⁸ Meanwhile, if both electrodes are moved together—changing the reference value of the electrostatic potential—we will obtain different pH values inside the system and in the reservoir. With such a definition, the system's pH will be different from that of the reservoir but will be the same as that of an isolated canonical system. Whichever definition of pH is chosen, one needs to know the Donnan potential in order to calculate the titration isotherms of isolated (canonical) systems using semi-grand canonical simulations. The “standard” cpH simulation methods do not allow us to calculate titration isotherms for isolated systems. One must either use canonical reactive MC—with Widom particle insertion, which is very inaccurate even for intermediate to high values—or the approach presented in this Communication, which is accurate for any pH.

This work was partially supported by the CNPq, the CAPES, and the National Institute of Science and Technology Complex Fluids (INCT-FCx).

AUTHOR DECLARATIONS

Conflict of Interest

The authors have no conflicts to disclose.

Author Contributions

Yan Levin: Conceptualization (lead); Supervision (lead); Writing – original draft (equal); Writing – review & editing (equal). **Amin Bakhshandeh:** Data curation (equal); Software (equal); Writing – original draft (equal); Writing – review & editing (equal).

DATA AVAILABILITY

The data that support the findings of this study are available within the article.

APPENDIX A: DETAILS FOR THE LIMITING PROCEDURE FOR SINGULAR TERM OF ELECTROSTATIC POTENTIAL

The electrostatic potential inside the simulation cell is

$$\begin{aligned} \phi(\mathbf{r}) = & \sum_{\mathbf{k}=0}^{\infty} \sum_{j=1}^N \frac{4\pi q_j}{\epsilon_w V |\mathbf{k}|^2} \exp \left[-\frac{|\mathbf{k}|^2}{4\kappa_e^2} + i\mathbf{k} \cdot (\mathbf{r} - \mathbf{r}_j) \right] \\ & + \sum_{j=1}^N \sum_n q_j \frac{\text{erfc}(\kappa_e |\mathbf{r} - \mathbf{r}_j - L\mathbf{n}|)}{\epsilon_w |\mathbf{r} - \mathbf{r}_j - L\mathbf{n}|} \\ & + \frac{1}{V} \sum_{\mathbf{k}=0}^{\infty} \tilde{\phi}_b(\mathbf{k}) \exp [i\mathbf{k} \cdot \mathbf{r}], \end{aligned} \quad (\text{A1})$$

where $V = L^3$ is the volume of the cubic simulation cell, $Q_t = \sum_i q_i$, and

$$\tilde{\phi}_b(\mathbf{k}) = -\frac{4\pi Q_t}{\epsilon_w V} \frac{\int_V e^{-i\mathbf{k}\cdot\mathbf{r}} d^3r}{k^2} \quad (\text{A2})$$

is the Fourier transform of the background potential. Note that the integral in Eq. (A2) vanishes for all \mathbf{k} , except for $\mathbf{k} = 0$, so that we can define the singular part of the background potential $\phi_{b,s}$ as $\tilde{\phi}_b(\mathbf{k}) \equiv \tilde{\phi}_{b,s} \delta_{\mathbf{k}0}$, where we have defined the Kronecker delta for the zero mode, $\delta_{\mathbf{k}0}$. As $\mathbf{k} \rightarrow 0$, we can expand the singular part around $\mathbf{k} = 0$,

$$\tilde{\phi}_{b,s} = -\frac{4\pi Q_t}{\epsilon_w V} \frac{\int_V (1 - i\mathbf{k} \cdot \mathbf{r} - \frac{1}{2}(\mathbf{k} \cdot \mathbf{r})^2 + \dots) d^3r}{k^2}. \quad (\text{A3})$$

The leading order terms in k are

$$\tilde{\phi}_{b,s} = -\frac{4\pi Q_t}{\epsilon_w k^2} + \frac{4\pi Q_t}{\epsilon_w k^2 V} \int_V i\mathbf{k} \cdot \mathbf{r} d^3r + \frac{2\pi Q_t}{\epsilon_w V k^2} \int_V (\mathbf{k} \cdot \mathbf{r})^2 d^3r, \quad (\text{A4})$$

with the higher order terms vanishing in the limit $\mathbf{k} \rightarrow 0$. We note that the limit $\mathbf{k} \rightarrow 0$ corresponds to a large distance behavior of the electrostatic potential. To clearly see how the divergence scales with the size of the macroscopic crystal, L_{cr} , produced by the periodic replication of simulation cell [see Fig. (1)], we introduce a “crystal” delta function as follows:

$$\begin{aligned} \delta_{cr}(\mathbf{k}) &= \frac{1}{(2\pi)^3} \prod_{i=1}^3 \int_{-L_{cr}/2}^{L_{cr}/2} e^{ik_i p_i} dp_i \\ &= \frac{1}{\pi^3} \prod_{i=1}^3 \frac{\sin(k_i L_{cr}/2)}{k_i}. \end{aligned} \quad (\text{A5})$$

In the limit $L_{cr} \rightarrow \infty$, $\delta_{cr}(\mathbf{k})$ becomes the Dirac delta function. The crystal $\delta_{cr}(\mathbf{k})$ regularizes the divergence and allows us to study the $\mathbf{k} \rightarrow 0$ limit.⁵⁰ In particular,

$$\lim_{\mathbf{k} \rightarrow 0} \frac{k_i k_j}{k^2} = \int \delta_{cr}(\mathbf{k}) \frac{k_i k_j}{k^2} d^3k = \frac{1}{3} \delta_{ij}, \quad (\text{A6})$$

where δ_{ij} is the Kronecker delta. The last equality follows from the direct use of the representation of $\delta_{cr}(\mathbf{k})$, Eq. (A5), followed by the $L_{cr} \rightarrow \infty$ limit,⁵⁰ or simply from the observation of symmetry. Similarly,

$$\lim_{\mathbf{k} \rightarrow 0} \frac{k_i}{k^2} = \int \delta_{cr}(\mathbf{k}) \frac{k_i}{k^2} d^3k = 0, \quad (\text{A7})$$

since $\delta_{cr}(\mathbf{k})$ is an even function of all k_i . Using Eq. (A7), we see that the second term of Eq. (A4) vanishes and the last term becomes

$$\frac{2\pi Q}{3\epsilon_w V} \int_V (x^2 + y^2 + z^2) dx dy dz = \frac{\pi Q L^2}{6\epsilon_w} \quad (\text{A8})$$

so that

$$\tilde{\phi}_{b,s} = -\frac{4\pi Q_t}{\epsilon_w k^2} + \frac{\pi Q_t L^2}{6\epsilon_w}. \quad (\text{A9})$$

We now expand the first term of Eq. (A1) around $\mathbf{k} = 0$. The singular terms are

$$\frac{4\pi}{V\epsilon_w k^2} \sum_{j=1}^N q_j - \frac{\pi}{\epsilon_w V \kappa_e^2} \sum_{j=1}^N q_j + \frac{4\pi}{V\epsilon_w} \sum_{j=1}^N q_j \frac{i\mathbf{k} \cdot (\mathbf{r} - \mathbf{r}_j)}{|\mathbf{k}|^2} - \frac{2\pi}{V\epsilon_w} \sum_{j=1}^N q_j \frac{[\mathbf{k} \cdot (\mathbf{r} - \mathbf{r}_j)]^2}{|\mathbf{k}|^2}, \quad (\text{A10})$$

which, using Eqs. (A7) and (A6), simplify to

$$\frac{4\pi Q_t}{\epsilon_w k^2 V} - \frac{\pi Q_t}{\epsilon_w V \kappa_e^2} - \frac{2\pi}{3V\epsilon_w} \sum_{j=1}^N q_j^i (\mathbf{r} - \mathbf{r}_j)^2. \quad (\text{A11})$$

Meanwhile, the expansion of the last term of Eq. (A1) around $\mathbf{k} = 0$, with the help of Eq. (A9), results in

$$- \frac{4\pi Q_t}{\epsilon_w k^2 V} + \frac{\pi Q_t}{6\epsilon_w L} + \frac{2\pi Q_t r^2}{3V\epsilon_w}. \quad (\text{A12})$$

Combining everything, we see that the diverging $1/k^2$ terms cancel out and we obtain the electrostatic potential inside the simulation cell,

$$\begin{aligned} \varphi(\mathbf{r}) = & \sum_{\mathbf{k} \neq 0} \sum_{j=1}^N \frac{4\pi q_j}{\epsilon_w V |\mathbf{k}|^2} \exp\left[-\frac{|\mathbf{k}|^2}{4\kappa_e^2} + i\mathbf{k} \cdot (\mathbf{r} - \mathbf{r}_j)\right] \\ & + \sum_{j=1}^N \sum_n q_j \frac{\text{erfc}(\kappa_e |\mathbf{r} - \mathbf{r}_j - L\mathbf{n}|)}{\epsilon_w |\mathbf{r} - \mathbf{r}_j - L\mathbf{n}|} \\ & - \frac{\pi Q_t}{\epsilon_w V \kappa_e^2} + \frac{4\pi}{3\epsilon_w V} \mathbf{r} \cdot \mathbf{M} - \frac{2\pi}{3\epsilon_w V} \sum_i q_i r_i^2 + \frac{\pi Q_t}{6\epsilon_w L}. \end{aligned} \quad (\text{A13})$$

APPENDIX B: REAL SPACE DERIVATION OF THE BETHE POTENTIAL INSIDE A CELL WITH A NEUTRALIZING BACKGROUND

The electrostatic potential, Eq. (A13), is invariant with respect to κ_e . In the limit $\kappa_e \rightarrow \infty$, the sum over erfc vanishes, and the electrostatic potential inside the cell can be written in terms of only the Fourier components. It is clear then that

$$\frac{1}{V} \int_V \varphi(\mathbf{r}) d^3 \mathbf{r} = \phi_B. \quad (\text{B1})$$

Following Bethe, we can also calculate this as the mean potential over the whole spherical crystal of radius $V_{cr} = 4\pi R^3/3$,

$$\phi_B = \frac{1}{\epsilon_w V_{cr}} \int_{V_{cr}} \int_{V_{cr}} \frac{\rho_q(\mathbf{r}')}{|\mathbf{r}' - \mathbf{r}|} d^3 \mathbf{r}' d^3 \mathbf{r}. \quad (\text{B2})$$

Interchanging the orders of integration, the integral over \mathbf{r} is the potential at position \mathbf{r}' inside a uniformly charged sphere of unit charge density, which can be easily obtained from the solution of Poisson equation,

$$\int_{V_{cr}} \frac{1}{|\mathbf{r}' - \mathbf{r}|} d^3 \mathbf{r} = \frac{2\pi}{3} (3R^2 - r'^2). \quad (\text{B3})$$

The average potential inside the simulation cell is then

$$\phi_B = \frac{2\pi}{3V} \int_V (3R^2 - r'^2) \rho_q(\mathbf{r}') d^3 \mathbf{r}' = -\frac{2\pi}{3V} \int_V r'^2 \rho_q(\mathbf{r}') d^3 \mathbf{r}', \quad (\text{B4})$$

where in the last equality, we have used the total ions + sites + background charge neutrality inside the cell. Finally, substituting $\rho_q(\mathbf{r}) = \sum_i q_i \delta(\mathbf{r} - \mathbf{r}_i) - \frac{Q_t}{V}$ into the above-mentioned equation, we obtain

$$\phi_B = -\frac{2\pi}{3\epsilon_w V} \sum_i q_i r_i^2 + \frac{\pi Q_t}{6\epsilon_w L}. \quad (\text{B5})$$

REFERENCES

- Y. Avni, R. Podgornik, and D. Andelman, "Critical behavior of charge-regulated macro-ions," *J. Chem. Phys.* **153**, 024901 (2020).
- D. Prusty, R. J. Nap, I. Szleifer, and M. Olvera de la Cruz, "Charge regulation mechanism in end-tethered weak polyampholytes," *Soft Matter* **16**, 8832–8847 (2020).
- R. Podgornik, "General theory of charge regulation and surface differential capacitance," *J. Chem. Phys.* **149**, 104701 (2018).
- T. Nishio, "Monte Carlo studies on potentiometric titration of (carboxymethyl)cellulose," *Biophys. Chem.* **57**, 261–267 (1996).
- Y. Avni, D. Andelman, and R. Podgornik, "Charge regulation with fixed and mobile charged macromolecules," *Curr. Opin. Electrochem.* **13**, 70–77 (2019).
- R. Lunkad, A. Murmiliuk, Z. Tošner, M. Štěpánek, and P. Košovan, "Role of pKA in charge regulation and conformation of various peptide sequences," *Polymers* **13**, 214 (2021).
- F. L. B. da Silva and B. Jönsson, "Polyelectrolyte–protein complexation driven by charge regulation," *Soft Matter* **5**, 2862–2868 (2009).
- T. Curk and E. Luijten, "Charge regulation effects in nanoparticle self-assembly," *Phys. Rev. Lett.* **126**, 138003 (2021).
- M. Lund, T. Åkesson, and B. Jönsson, "Enhanced protein adsorption due to charge regulation," *Langmuir* **21**, 8385–8388 (2005).
- R. J. Nap, A. L. Božič, I. Szleifer, and R. Podgornik, "The role of solution conditions in the bacteriophage PP7 capsid charge regulation," *Biophys. J.* **107**, 1970–1979 (2014).
- M. Lund, "Electrostatic chameleons in biological systems," *J. Am. Chem. Soc.* **132**, 17337–17339 (2010).
- A. Majej, M. Bier, R. Blossey, and R. Podgornik, "Charge regulation radically modifies electrostatics in membrane stacks," *Phys. Rev. E* **100**, 050601 (2019).
- R. Netz, "Charge regulation of weak polyelectrolytes at low- and high-dielectric-constant substrates," *J. Phys.: Condens. Matter* **15**, S239 (2002).
- J. N. Israelachvili, "Units, symbols, useful quantities and relations," in *Intermolecular and Surface Forces*, 3rd ed. (Academic Press, San Diego, CA, 2011).
- S. H. Behrens, D. I. Christl, R. Emmerzael, P. Schurtenberger, and M. Borkovec, "Charging and aggregation properties of carboxyl latex particles: Experiments versus DLVO theory," *Langmuir* **16**, 2566–2575 (2000).
- I. Palaia, A. Goyal, E. Del Gado, L. Šamaj, and E. Trizac, "Like-charge attraction at the nanoscale: Ground-state correlations and water destructuring," *J. Phys. Chem. B* **126**, 3143–3149 (2022).
- M. Lund and B. Jönsson, "Charge regulation in biomolecular solution," *Q. Rev. Biophys.* **46**, 265–281 (2013).
- M. Lund and B. Jönsson, "On the charge regulation of proteins," *Biochemistry* **44**, 5722–5727 (2005).
- J. Landsgesell, L. Nová, O. Rud, F. Uhlík, D. Sean, P. Hebbeker, C. Holm, and P. Košovan, "Simulations of ionization equilibria in weak polyelectrolyte solutions and gels," *Soft Matter* **15**, 1155–1185 (2019).
- N. A. Pérez-Chávez, A. G. Albesa, and G. S. Longo, "Thermodynamic theory of multiresponsive microgel swelling," *Macromolecules* **54**, 2936–2947 (2021).
- Y. Burak and R. R. Netz, "Charge regulation of interacting weak polyelectrolytes," *J. Phys. Chem. B* **108**, 4840–4849 (2004).
- T. Hiemstra, W. v. Riemsdijk, and M. Bruggenwert, "Proton adsorption mechanism at the gibbsite and aluminium oxide solid/solution interface," *Neth. J. Agric. Sci.* **35**, 281–293 (1987).

- ²³T. Hiemstra and W. Van Riemsdijk, "Physical chemical interpretation of primary charging behaviour of metal (hydr)oxides," *Colloids Surf.* **59**, 7–25 (1991).
- ²⁴A. Bakhshandeh, A. P. Dos Santos, and Y. Levin, "Interaction between charge-regulated metal nanoparticles in an electrolyte solution," *J. Phys. Chem. B* **124**, 11762–11770 (2020).
- ²⁵A. Bakhshandeh, D. Frydel, and Y. Levin, "Theory of charge regulation of colloidal particles in electrolyte solutions," *Langmuir* **38**, 13963 (2022).
- ²⁶Y. Levin, "Electrostatic correlations: From plasma to biology," *Rep. Prog. Phys.* **65**, 1577 (2002).
- ²⁷Y. Levin and M. E. Fisher, "Criticality in the hard-sphere ionic fluid," *Physica A* **225**, 164–220 (1996).
- ²⁸C. Labbez and B. Jönsson, *A New Monte Carlo Method for the Titration of Molecules and Minerals* (Springer, 2006), pp. 66–72.
- ²⁹C. Labbez, B. Jönsson, M. Skarba, and M. Borkovec, "Ion–ion correlation and charge reversal at titrating solid interfaces," *Langmuir* **25**, 7209–7213 (2009).
- ³⁰Y. Levin and A. Bakhshandeh, "Comment on "Simulations of ionization equilibria in weak polyelectrolyte solutions and gels" by J. Landsgesell, L. Nová, O. Rud, F. Uhlík, D. Sean, P. Hebbeker, C. Holm and P. Košovan, *Soft Matter*, 2019, 15, 1155–1185," *Soft Matter* **19**, 3519–3521 (2023).
- ³¹W. Smith and B. Triska, "The reaction ensemble method for the computer simulation of chemical and phase equilibria. I. Theory and basic examples," *J. Chem. Phys.* **100**, 3019–3027 (1994).
- ³²J. K. Johnson, A. Z. Panagiotopoulos, and K. E. Gubbins, "Reactive canonical Monte Carlo: A new simulation technique for reacting or associating fluids," *Mol. Phys.* **81**, 717–733 (1994).
- ³³C.-Y. Leung, L. C. Palmer, S. Kewalramani, B. Qiao, S. I. Stupp, M. Olvera de la Cruz, and M. J. Bedzyk, "Crystalline polymorphism induced by charge regulation in ionic membranes," *Proc. Natl. Acad. Sci. U. S. A.* **110**, 16309–16314 (2013).
- ³⁴G. M. Ong, A. Gallegos, and J. Wu, "Modeling surface charge regulation of colloidal particles in aqueous solutions," *Langmuir* **36**, 11918–11928 (2020).
- ³⁵H. Wennerström, B. Jönsson, and P. Linse, "The cell model for polyelectrolyte systems. Exact statistical mechanical relations, Monte Carlo simulations, and the Poisson–Boltzmann approximation," *J. Chem. Phys.* **76**, 4665–4670 (1982).
- ³⁶J. Landsgesell, P. Hebbeker, O. Rud, R. Lunkad, P. Košovan, and C. Holm, "Grand-reaction method for simulations of ionization equilibria coupled to ion partitioning," *Macromolecules* **53**, 3007–3020 (2020).
- ³⁷T. Curk, J. Yuan, and E. Luijten, "Accelerated simulation method for charge regulation effects," *J. Chem. Phys.* **156**, 044122 (2022).
- ³⁸T. Bollhorst, K. Rezwan, and M. Maas, "Colloidal capsules: Nano- and microcapsules with colloidal particle shells," *Chem. Soc. Rev.* **46**, 2091–2126 (2017).
- ³⁹F. G. Donnan, "Theorie der membrangleichgewichte und membranpotentiale bei vorhandensein von nicht dialysierenden elektrolyten. Ein beitrag zur physikalisch-chemischen physiologie," *Z. Elektrochem. Angew. Phys. Chem.* **17**, 572–581 (1911).
- ⁴⁰S. Barr and A. Panagiotopoulos, "Grand-canonical Monte Carlo method for Donnan equilibria," *Phys. Rev. E* **86**, 016703 (2012).
- ⁴¹R. v. Roij, "Defying gravity with entropy and electrostatics: Sedimentation of charged colloids," *J. Phys.: Condens. Matter* **15**, S3569 (2003).
- ⁴²A. P. Phillipse, "Remarks on the Donnan condenser in the sedimentation–diffusion equilibrium of charged colloids," *J. Phys.: Condens. Matter* **16**, S4051 (2004).
- ⁴³P. Warren, "Electrifying effects in colloids," *Nature* **429**, 822 (2004).
- ⁴⁴T. Eckert, M. Schmidt, and D. de las Heras, "Sedimentation of colloidal plate-sphere mixtures and inference of particle characteristics from stacking sequences," *Phys. Rev. Res.* **4**, 013189 (2022).
- ⁴⁵M. Sullivan, K. Zhao, C. Harrison, R. H. Austin, M. Megens, A. Hollingsworth, W. B. Russel, Z. Cheng, T. Mason, and P. Chaikin, "Control of colloids with gravity, temperature gradients, and electric fields," *J. Phys.: Condens. Matter* **15**, S11 (2002).
- ⁴⁶E. R. Smith, "Electrostatic energy in ionic crystals," *Proc. R. Soc. London, Ser. A* **375**, 475–505 (1981).
- ⁴⁷D. Frenkel and B. Smit, *Understanding Molecular Simulation: From Algorithms to Applications* (Elsevier, 2001), Vol. 1.
- ⁴⁸M. P. Allen and D. J. Tildesley, *Computer Simulation of Liquids* (Oxford University Press, 2017).
- ⁴⁹Z. Hu, "Infinite boundary terms of Ewald sums and pairwise interactions for electrostatics in bulk and at interfaces," *J. Chem. Theory Comput.* **10**, 5254–5264 (2014).
- ⁵⁰A. P. dos Santos, M. Girotto, and Y. Levin, "Simulations of Coulomb systems with slab geometry using an efficient 3d Ewald summation method," *J. Chem. Phys.* **144**, 144103 (2016).
- ⁵¹S. Yi, C. Pan, and Z. Hu, "Note: A pairwise form of the Ewald sum for non-neutral systems," *J. Chem. Phys.* **147**, 126101 (2017).
- ⁵²R. Euwema and G. Surratt, "The absolute positions of calculated energy bands," *J. Phys. Chem. Solids* **36**, 67–71 (1975).
- ⁵³S. De Leeuw and J. Perram, "Computer simulation of ionic systems. Influence of boundary conditions," *Physica A* **107**, 179–189 (1981).
- ⁵⁴J. S. Høye and E. Lomba, "Mean spherical approximation (MSA) for a simple model of electrolytes. I. Theoretical foundations and thermodynamics," *J. Chem. Phys.* **88**, 5790–5797 (1988).
- ⁵⁵N. F. Carnahan and K. E. Starling, "Equation of state for nonattracting rigid spheres," *J. Chem. Phys.* **51**, 635–636 (1969).
- ⁵⁶A. Bakhshandeh, D. Frydel, and Y. Levin, "Reactive Monte Carlo simulations for charge regulation of colloidal particles," *J. Chem. Phys.* **156**, 014108 (2022).
- ⁵⁷E. A. Guggenheim, "On the conception of electrical potential difference between two phases. II," *J. Phys. Chem.* **34**, 1540–1543 (1930).
- ⁵⁸S. Craxford, O. Gatty, and T. Teorell, "XCV. A note on surface ph," *London, Edinburgh Dublin Philos. Mag. J. Sci.* **25**, 1061–1066 (1938).